Journal of Virology

The Murine Model for Hantaan Virus-Induced Lethal Disease Shows Two Distinct Paths in Viral Evolutionary Trajectory with and without Ribavirin Treatment

Dong-Hoon Chung, Åke Västermark, Jeremy V. Camp, Ryan McAllister, Susanna K. Remold, Yong-Kyu Chu, Carl Bruder and Colleen B. Jonsson

***J. Virol.* 2013, 87(20):10997. DOI: 10.1128/JVI.01394-13.**
Published Ahead of Print 31 July 2013.

JVI Journals.ASM.org

The Murine Model for Hantaan Virus-Induced Lethal Disease Shows Two Distinct Paths in Viral Evolutionary Trajectory with and without Ribavirin Treatment

Dong-Hoon Chung,[a,b] Åke Västermark,[c] Jeremy V. Camp,[a] Ryan McAllister,[d] Susanna K. Remold,[e] Yong-Kyu Chu,[b] Carl Bruder,[b] Colleen B. Jonsson[a,b,d]

Department of Microbiology and Immunology, University of Louisville, Louisville, Kentucky, USA[a]; Center for Predictive Medicine for Biodefense and Emerging Infectious Diseases, University of Louisville, Louisville, Kentucky, USA[b]; Department of Molecular Biology, University of California at San Diego, La Jolla, California, USA[c]; Department of Pharmacology and Toxicology, University of Louisville, Louisville, Kentucky, USA[d]; Department of Biology, University of Louisville, Louisville, Kentucky, USA[e]

***In vitro*, ribavirin acts as a lethal mutagen in Hantaan virus (HTNV)-infected Vero E6 cells, resulting in an increased mutation load and viral population extinction. In this study, we asked whether ribavirin treatment in the lethal, suckling mouse model of HTNV infection would act similarly. The HTNV genomic RNA (vRNA) copy number and infectious virus were measured in lungs of untreated and ribavirin-treated mice. In untreated, HTNV-infected mice, the vRNA copy number increased for 10 days postinfection (dpi) and thereafter remained constant through 26 dpi. Surprisingly, in ribavirin-treated, HTNV-infected mice, vRNA levels were similar to those in untreated mice between 10 and 26 dpi. Infectious virus levels, however, were different: in ribavirin-treated mice, the amount of infectious HTNV was significantly decreased relative to that in untreated mice, suggesting that ribavirin reduced the specific infectivity of the virus (amount of infectious virus produced per vRNA copy). Mutational analysis revealed a ribavirin-associated elevation in mutation frequency in HTNV vRNA similar to that previously reported *in vitro*. Codon-based analyses of rates of nonsynonymous (*dN*) and synonymous (*dS*) substitutions in the S segment revealed a positive selection for codons within the HTNV N protein gene in the ribavirin-treated vRNA population. In contrast, the vRNA population in untreated, HTNV-infected mice showed a lower level of diversity, reflecting purifying selection for the wild-type genome. In summary, these experiments show two different evolutionary paths that *Hantavirus* may take during infection in a lethal murine model of disease, as well as the importance of the *in vivo* host environment in the evolution of the virus, which was not apparent in our prior *in vitro* model system.**

Hantaviruses, which are members of the genus *Hantavirus* in the family *Bunyaviridae*, provide an exceptionally well-characterized model system for the study of zoonotic RNA virus emergence, disease, and evolution (1). Hantaviruses have three negative-sense, single-stranded RNA segments (S, M, and L), which encode the nucleocapsid (N), two glycoproteins (G_N and G_C), and the RNA-dependent RNA polymerase (RdRp, or L protein), respectively (2, 3). In nature, hantaviruses are harbored by wild rodent reservoirs, in which they do not cause any apparent disease. Upon spillover to nonreservoir hosts such as humans, however, they can cause two serious illnesses, i.e., hemorrhagic fever with renal syndrome (HFRS) and hantavirus pulmonary syndrome (HPS), with resulting lethality rates ranging from 1 to 50% depending on the viral strain (1, 4). Laboratory animal models of hantaviruses have proven useful for basic research to study infection and virulence (5–8) and for the discovery of therapeutics and potential vaccine candidates (9–14). For example, the well-established lethal, suckling mouse model of Hantaan virus (HTNV) infection demonstrated ribavirin's therapeutic efficacy (12) and provided the impetus for clinical studies of its efficacy in humans (11, 13). Ribavirin was recently shown to have efficacy *in vivo* in the lethal hamster model of Andes virus, a New World hantavirus (14). Clinical studies of intravenous ribavirin treatment of HFRS in human cases caused by HTNV have shown efficacy, with a decrease in occurrence of oliguria severity of renal insufficiency (13). No other treatment is available for either disease.

The study of an antiviral both *in vitro* and in an animal model of disease progression is important for a complete understanding of its mechanism of action and potential for selecting for drug resistance or lethal mutagenesis (15–18). Lethal mutagenesis is a chemotherapeutic strategy in which one uses a viral mutagen to promote the lethal accumulation of mutations in an RNA viral genome. Ribavirin is a potent, broad-spectrum antiviral for many RNA and DNA viruses *in vitro* and *in vivo* (19). The antiviral activity against several viruses is due to its ability to competitively inhibit inosine monophosphate dehydrogenase (IMPDH) (20, 21), a key enzyme in the *de novo* synthesis of GTP. Additional targets for its antiviral activity have been shown, including capping (22), translation efficiency of viral mRNA (23), and a direct suppressive effect on the viral polymerase activity (24–26). Ribavirin can also act as a potent RNA virus mutagen for several RNA viruses and can cause error-prone replication (18, 27–30). In addition to targeting the purine metabolic pathway and viral enzymes, recent studies suggest that ribavirin may act by promoting a type 1 immune response (31). Specifically, Kobayashi et al. showed that ribavirin can downmodulate interleukin-10 (IL-10)-producing Treg 1 cells, which could inhibit the conversion of

Received 23 May 2013 **Accepted** 23 July 2013
Published ahead of print 31 July 2013
Address correspondence to Colleen B. Jonsson, cbjons01@louisville.edu.
D.-H.C., Å.V., J.V.C., and R.M. contributed equally to this article.

doi:10.1128/JVI.01394-13

$CD4^+$ $CD25^-$ $FOXP3^-$ naive T cells into $CD4^+$ $CD25^+$ $FOXP3^+$ adaptive Treg cells to maintain Th1 cell activity (32). The role of the ribavirin-induced immune response in acting as a selective pressure on hantaviral population and evolution has not yet been addressed.

In vitro, we have shown direct effects of ribavirin on HTNV through the host IMPDH and viral replication (33), which correlates with an increase in mutations in the viral RNA (vRNA) genome (34, 35). Our studies on the mechanism of action of ribavirin's potent antiviral activity have also provided insight into the standing genetic variation and population structure of HTNV (34, 35). These studies revealed an increase in the mutation frequency in the viral population, after which the mutation frequency did not correlate with a dose-dependent decrease in the level of viral RNA, PFU, or [RTP]/[GTP]. Intriguingly, even at the highest concentrations of ribavirin-treated cells, the proportion of HTNV wild-type sequences never dropped below 60% for the target S-segment sequence used in sampling. These studies suggested that HTNV could not survive past a critical mutational burden or lethal threshold.

Based on the findings of our prior studies (34, 35), we sought to test whether mice infected with HTNV and treated with ribavirin would show an increase in mutation frequency and demonstrate a lethal extinction threshold. Specifically, would ribavirin cause extinction as revealed by an increase in viral mutation rate followed by a steady decrease in titer *in vivo*? We found that, surprisingly, untreated, HTNV-infected mice showed an overall apparent decrease in mutational frequency compared to the previous mutational frequencies measured for the HTNV seed stock in Vero E6 cells (34, 35). In contrast, ribavirin-treated, HTNV-infected mice showed an increased mutational load. Both populations showed a reduction in specific infectivity over time. These studies show, for the first time, two distinct evolutionary trajectories for HTNV within a lethal mouse model of disease in the presence and absence of ribavirin, as well as evidence for positive selection not previously observed *in vitro*. In the ribavirin-treated vRNA population, analyses of rates of nonsynonymous (*dN*) and synonymous (*dS*) substitutions in the S segment revealed a positive selection for codons within the HTNV N protein gene, while untreated, HTNV-infected mice showed purifying selection. Furthermore, in contrast to our prior *in vitro* studies (34, 35), the increased mutational load did not lead to lethal extinction. Intriguingly, viral RNA levels remained high in both untreated and treated populations, with a decrease in the level of infectious virus over time. The levels of infectious virus produced by the two populations, however, were statistically significantly different, reflecting a difference in the selective pressure by the host with and without ribavirin. Importantly, these data reveal that while the virus populations within the ribavirin-treated, HTNV-infected mice had a larger proportion of deleterious mutations leading to a smaller number of infectious particles, they harnessed the increased mutation rate to also achieve genetic changes that improved their survival over that of the wild type. Finally, while a direct analysis of the potential for ribavirin-induced immune responses as an added selective pressure was not possible in the context of this experiment, the immune system of the suckling mouse model was assessed at the time point for ribavirin treatment, which was 11 days postnatal (dpn) or 10 days postinfection (dpi). These studies showed a responsive innate immune system in these young mice.

MATERIALS AND METHODS

Cells and virus. Vero E6 cells (CRL-1586; ATCC) were propagated and used for production of HTNV strain 76-118 and measurement of virus in tissue samples. Cells were cultured in Dulbecco's modified Eagle's medium (DMEM; Invitrogen) supplemented with 10% fetal bovine serum (FBS), 1% penicillin-streptomycin, and 1% L-glutamine (Sigma). The titers of virus in the seed stock and in animal tissues were measured by determining the numbers of PFU per ml, using an agarose overlay method as described previously (36).

Animal study. ICR suckling mice (Harlan, Prattville, AL) were used for all animal studies and were individually identified by tattoo. Pregnant mice were housed singly with their pups in solid-bottom polycarbonate cages on stainless steel racks in an environmentally monitored, well-ventilated room. Bedding (P. J. Murphy Forest Products, Inc., Montville, NJ) was used in the bottom of the cages. Dams were fed on certified rodent diet 5002 (PMI Feeds, Inc., St. Louis, MO), and tap water was provided *ad libitum* during the study periods. Procedures used in this study were designed to conform to accepted practices and to minimize or avoid causing pain, distress, or discomfort in the animals and were approved by the Institutional Animal Care and Use Committee (IACUC) at Southern Research Institute.

Animals were monitored for a 26-day period following intracranial (i.c.) challenge with HTNV (strain 76-118). On day 0, each mouse in group 1 received 10 μl DMEM and each mouse in groups 2 and 3 received 10 μl of 1×10^3 PFU HTNV diluted in DMEM. Beginning at 11 dpn or 10 dpi, each mouse was treated with ribavirin (MP Biomedical, Inc.) via the intraperitoneal (i.p.) route at 5 μl/g of body weight (50 mg/kg of body weight) for 15 days. All mice were observed twice daily throughout the study periods for signs of morbidity and mortality and for body weight, and detailed observations were recorded daily beginning at −1 dpi.

Isolation of total RNA, cDNA synthesis, and real-time RT-PCR. Briefly, total RNAs from infected tissues were homogenized and extracted with TRIzol (Invitrogen), and 0.5 μg of total RNA was subjected to a reverse transcription (RT) reaction with SuperScript III reverse transcriptase (Invitrogen). The HTNV S-segment vRNA copy number within virus-infected mouse tissues was measured with a real-time RT-PCR assay using the comparative threshold cycle method, i.e., $2^{-\Delta\Delta CT}$ method (33, 34). Real-time PCRs were performed in triplicate for each sample and were prepared with TaqMan universal PCR master mix (Applied Biosystems).

Sequencing and phylogenetic analyses. cDNAs were cloned and analyzed for each lung tissue as described previously (34). Briefly, cDNA prepared as described above was amplified by a PCR using Phusion High-Fidelity DNA polymerase (Finnzymes Oy, Finland) following the manufacturer's protocols. Primers HS24 (forward primer; 5′-TACTAGAACA ACGATGGCAACTATG-3′) and HS1336 (reverse primer; 5′-GTGCAAA TATGATTGATAATGATTCAGTAG-3′) were used to amplify the open reading frame of N within the S-segment gene. The amplified product was cloned into the pCR-4 plasmid (Topo cloning kits for sequencing; Invitrogen) after A tailing by using *Taq* polymerase (Promega). On average, 96 colonies per lung were subjected to colony PCR using the M13 forward and M13 reverse primers (34). As a control, the background mutation frequency (inherent in the amplification process) was measured using the same enzymes and plasmid DNA encoding the HTNV S-segment cDNA.

SeqScape 2.1 was used to generate the open reading frame (from codons 19 to 430) of the plus strand of the HTNV S-segment forward and reverse sequences from each of the clones from each lung. The ABI file of each sequence was evaluated manually, and sequences with inconclusive nucleotides (nt) at any position, stop codons, or gaps were removed. Sequences were exported into fasta file format, aligned by ClustalW in Mega 5.1 (37), and compared to the published HTNV 76-118 sequence (GenBank accession number M14626) as well as other sequences to generate phylogenetic trees (38). Mutation frequencies for each sample were calculated from the alignment of individual cDNA sequences with that of HTNV 76-118. Phylogenetic analyses based on maximum likelihood or

TABLE 1 Groups, treatments, and sampling design

Group/treatment[a]	No. of mice at dpn/dpi:										Total no. of mice
	5/4	9/8	11/10	13/12	15/14	18/17	19/18	21/20	23/22	27/26	
Group 1/no virus (mock)			2		2		2				6
Group 2/HTNV	2	2	2	3	5	2	2		1	3	16
Group 3/HTNV and RBV				3	3	1		3		3	14

[a] RBV, ribavirin.

neighbor-joining programs were generated from the ClustalW alignments in Mega 5.1, with 1,000 bootstraps (37).

Ratio of nonsynonymous to synonymous substitution rates. The ClustalW alignments for the mock-treated and ribavirin-treated groups defined above were analyzed by the Web server Datamonkey (39). The sequence sets were analyzed by single-likelihood ancestor counting (SLAC), fixed-effects likelihood (FEL), internal fixed-effects likelihood (IFEL), mixed-effects model of evolution (MEME), and fast unbiased Bayesian approximation (FUBAR), using default settings (39). Datamonkey removed all identical sequences, which left 32 and 107 sequences that differed in the mock-treated and ribavirin-treated groups, respectively. Automatic model selection identified the HKY85 nucleotide substitution bias model.

Statistical analyses. Statistical analyses of virus loads from the animal study were performed using R, a language and environment for statistical computing and graphics (www.r-project.org/). A set of generalized linear models (GLM) were used to test the main effects of treatment (mock or ribavirin) and dpi on viral load (given by vRNA copy number, number of PFU, or number of PFU/vRNA copy) in mice. Full models including an interaction term were included in the goodness-of-fit assessments, and all simpler models were considered to define the accepted model used in interpretation of data. Only data from time points after the ribavirin course of treatment were included in the analysis (i.e., ≥12 dpi). Day 26 was not included in the analyses. Best-fit statistical models were selected using log-likelihood ratio estimates and the Akaike information criterion (AIC). In cases where single effects models were the best fit to explain the data, nonparametric statistical tests were used to describe the difference between groups. In all analyses, the type I error rate was set to an α level of 0.05.

RESULTS

Study design. To define the intrahost mutation frequency and population structure of HTNV following infection in mock- and ribavirin-treated, HTNV-infected mice, we employed a standard experimental design and lethal murine model of HTNV that is used to measure antiviral efficacy (Table 1) (12). One-day-old suckling mice were infected with 1,000 PFU of HTNV, and from 10 to 24 dpi, mice were treated once per day with 50 mg/kg of ribavirin. Mice were sacrificed as noted in Table 1, and lung tissues were harvested and flash frozen in liquid nitrogen. At the same time that this study was conducted, an efficacy study of an analog of ribavirin was conducted in parallel (40). The mean time to death (MTD) and percent survival in ribavirin-treated, HTNV-infected mice published as part of that study were 18.5 days and 35%, compared to 15.5 days and 10% survival for untreated, HTNV-infected mice (40). In the groups presented in Table 1, the mock-treated, HTNV-infected mice that survived to day 26 were moribund, and the virus was below the limit of detection by plaque assay. The day 26 time point was not included in our analyses.

Viral titers in lungs of untreated and ribavirin-treated mice. Lung tissue was harvested and analyzed for S-segment vRNA copy number by real-time RT-PCR and for number of PFU for both mock- and ribavirin-treated, HTNV-infected mice (Fig. 1). In the mock-treated group, the vRNA copy number increased through day 12 and remained fairly constant in the few mice that survived from days 14 to 23 (Fig. 1A). Similarly, in the ribavirin-treated group, the vRNA copy number remained steady from days 14 to 26. GLM testing and statistical comparison of vRNA levels (days 12 to 24) in the mock-treated and ribavirin-treated groups showed that they differed significantly (Wilcoxon rank sum test; $P = 0.035$). These data showed that the ribavirin-treated group had more vRNA copies on days 12 to 20 than the mock-treated, HTNV-infected mice.

In the mock-treated, HTNV-infected mice, viral titers measured by plaque assay increased through day 9 (Fig. 1B). After day 9, mock- and ribavirin-treated, HTNV-infected mice showed similar levels of PFU over time. GLM model fitting confirmed that the dpi-only model was the best fit to explain the variance in numbers of PFU, and analysis of variance (ANOVA) showed no significant effect of treatment (with or without ribavirin) on the number of PFU, controlling for dpi ($P = 0.84$).

We calculated and plotted the selective infectivity (number of PFU/vRNA copy) over time (Fig. 1C), as we have found this valuable for comparisons made across groups and experiments conducted *in vitro* (34). Analysis of the data by GLM showed that treatment only was the best model to explain the variation in the data. Therefore, we used a nonparametric Wilcoxon rank sum test to compare these two groups, ignoring changes over time, to determine if there was a difference in the PFU/vRNA ratio due to ribavirin treatment. These data suggest that the specific infectivity for the ribavirin-treated, HTNV-infected mice was lower than that for untreated mice ($P = 0.053$). A model of the probability density for each population is shown in Fig. 1D.

Intrahost genetic variation of HTNV in untreated and ribavirin-treated mice. Using a previously standardized approach to measure the mutation frequency of HTNV (34), estimates of nucleotide and amino acid (aa) mutation frequencies were made for each viral population in each mouse lung (Table 2). Briefly, total RNA was isolated, and S-segment cDNAs were PCR amplified, cloned, sequenced, and aligned using ClustalW. The region cloned was the open reading frame of the N protein. Changes from the master consensus (HTNV seed stock) were counted, and the estimated mutation frequency per 10,000 nucleotides or 3,333 amino acids is shown (Table 2). Our prior analyses for standardization of the method showed that an accurate assessment of mutation frequency is reached with a sample size of 48 clones for each sample, after which no change in the proportion of genetic variation or frequency is noted (34). The number of cDNAs examined for each mouse lung sample is shown in Table 2, after removal of sequences with stop codons, gaps, or poor sequence information. For this analysis, we used a total of 653 sequences for the ribavirin-treated, HTNV-infected group, among which 107 sequences

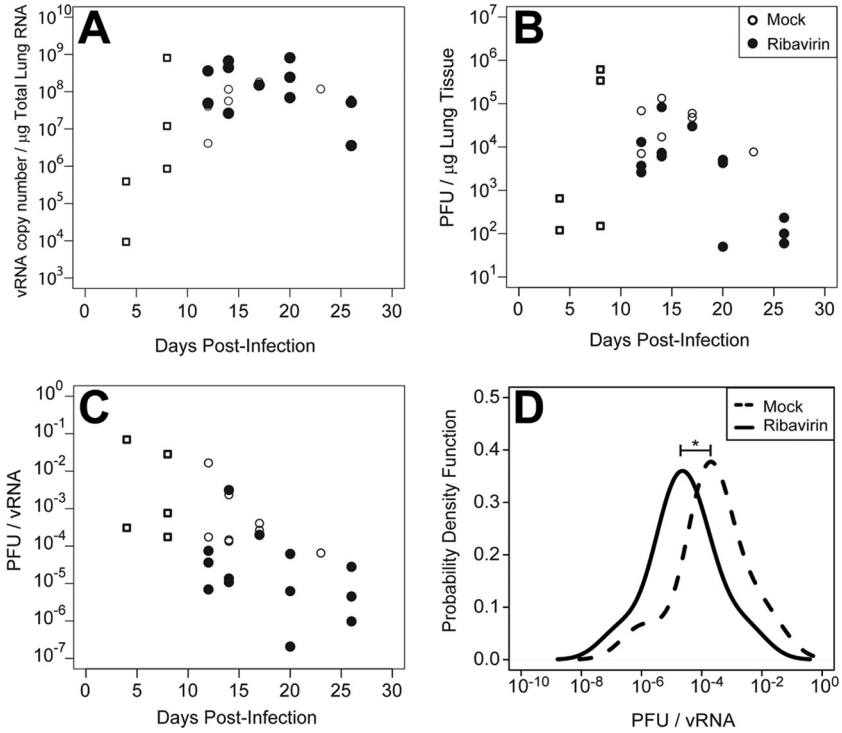

FIG 1 Viral RNA and infectious virus levels in lung tissues of untreated and ribavirin-treated, HTNV-infected mice. (A and B) Lung tissue was homogenized from each animal specimen and divided to measure the copy numbers of HTNV S-segment vRNA per g of tissue in mock-treated (open circles) and ribavirin-treated (solid circles), HTNV-infected mice (A) and the levels of infectious virus in lung tissue suspensions (numbers of PFU) (B). Some vRNA-positive samples were from animals that were moribund; infectious viruses from these animals were below the limit of detection in plaque assays and were eliminated from the subsequent analyses of selective infectivity. Open squares indicate untreated, HTNV-infected mice but are noted differently because statistical comparisons did not take these time points into consideration. (C) Selective infectivity (number of PFU per vRNA copy, based on grams of lung tissue) plotted by days postinfection for HTNV-infected mice that were treated with phosphate-buffered saline (PBS) or ribavirin from 10 to 25 dpi. (D) Smoothed histograms (probability density functions) of selective infectivities for both groups, i.e., HTNV-infected mice (dashed line) and HTNV-infected, ribavirin-treated mice (solid line). The Wilcoxon rank sum test showed that there was a significant reduction in the number of PFU/vRNA copy in ribavirin-treated mice, including only samples from 12 to 25 dpi (*, $P = 0.053$).

showed nt/aa differences from the consensus sequence. For the mock-treated, HTNV-infected group, we used a total of 408 sequences, among which 32 showed nt/aa differences.

On day 8 postinfection, the estimated standing genetic variation in the mock-treated animals ranged from 0.51 to 0.84 mutation per 10,000 nt (Table 2; Fig. 2). Our previous *in vitro* estimates show that HTNV has an estimated average mutation frequency of 1.1 to 1.4 mutations per 10,000 nt in Vero E6 cells (34). In the mock-treated mice, the mutation frequencies of the HTNV population showed a nearly 2-fold decrease (Fig. 2) ($P < 0.05$). On average, 0.5 mutation per 10,000 nt was estimated overall from days 8 to 23. In contrast, in HTNV-infected mice treated with ribavirin, the average mutation frequencies from days 12 to 20 (2.3/10,000 nt) or days 12 to 26 (1.8/10,000 nt) were 3- to 4-fold higher ($P < 0.05$) (Table 2; Fig. 2).

We further examined the mutational frequency of HTNV in mock-treated and ribavirin-treated mice by the specific infectivity, i.e., the number of PFU/vRNA copy (Fig. 3). The hatched line in Fig. 3A shows the mutation frequency of approximately 1.1 mutations per 10,000 nt measured *in vitro*. The graph shows a flattening of specific infectivity with increased genetic variation in the population (ribavirin-treated mice). For the mock-treated group, the specific infectivity falls below this mutation frequency, while more than half of the ribavirin points fall above this line (Fig. 3A). Analysis of these data by a probability density function showed that the mock-treated, HTNV-infected mice had a sharp narrow peak with decreased mutations, while the ribavirin-treated group had a broader and lower peak of distribution (Fig. 3B). Levene's test for equal variance showed that HTNV-infected, mock-treated mice had marginally significantly more variance than ribavirin-treated animals ($P = 0.067$) (Fig. 3B).

In Table 3, the amino acid changes from the consensus (HTNV 76-118) are presented for each mouse in each of the treatment groups by day. A larger number of amino acid changes (92 in total) was noted in the ribavirin-treated, HTNV-infected group than in the mock-treated group (16 in total). Of those amino acids with a change, 29/92 amino acids showed a gain or loss of negative/positive charge (Table 3). The distribution of amino acid changes along the protein shows some clustering (Fig. 4). The mock-treated group showed 13 of 16 changes in the first half of the N protein. The distribution of amino acid changes predominated throughout the N protein in the ribavirin-treated group. Interestingly, a greater percentage (42%) of those changed in the amino and carboxyl termini (first and last 110 aa) had changes in charge. In contrast, the central region had many fewer (20 to 30%) changes in charge.

Phylogenetic relationships of sequences. Nucleotide and amino acid alignments were made with 654 sequences from the

TABLE 2 Summary of mutation frequencies in mock- and ribavirin-treated, HTNV-infected mice

Treatment group and mouse ID	Day	No. of nt changes[a]	Total no. of cDNAs[b]	nt mutation frequency (per 10,000 nt)	aa mutation frequency (per 3,333 aa)
Mock-treated, HTNV-infected mice					
1007	8	7	48	1.18	0.67
1009	8	2	32	0.51	0.25
402	12	4	44	0.55	0.55
404	12	4	45	0.72	0.54
504	12	5	48	0.84	0.51
308	14	0	31	0	0
303	14	4	37	0.88	0.21
407	17	1	43	0.19	0.19
305	17	2	33	0.49	0
401	23	3	47	0.51	0
Total/avg[c]		31	408	0.61	0.42
Ribavirin-treated, HTNV-infected mice					
1012	12	11	43	2.1	1.13
1013	12	2	44	0.37	0.37
1201	12	4	42	0.77	0.77
1105	14	12	117	0.83	0.41
1112	14	4	40	0.81	0.61
1204	14	16	45	2.9	1.27
1102	17	2	35	0.46	0.46
1209	20	10	43	1.88	1.51
1208	20	4	15	2.16	2.16
1207	20	5	47	0.86	0.69
1109	26	23	42	4.4	3.27
1101	26	15	95	1.28	0.94
1110	26	27	45	4.85	3.24
Total/avg[c]		135	653	1.8	1.3

[a] Based on 1,236 nt of cDNA.
[b] Total number of cDNAs analyzed per mouse.
[c] Totals are shown for numbers of nt changes and cDNAs, and averages are shown for mutation frequencies.

ribavirin treatment group and 418 sequences from the mock treatment group. The consensus sequences from other strains and species of hantaviruses reported in GenBank were included in the alignment (GenBank numbers are available upon request). From the alignments, 546 of the 654 ribavirin treatment group sequences and 386 of the 418 sequences from the mock-treated group were identical. The best-scoring maximum likelihood trees for mock-treated (Fig. 5A) and ribavirin-treated (Fig. 5B) mice, with additional wild-type sequences from Hantaan viral strains, are presented. As predicted from the mutation frequencies, the number of sequences showing nucleotide differences (light blue) and bifurcation was greater in the ribavirin-treated group (Fig. 5B) than in the mock-treated group (Fig. 5A). Tests for positive selection are discussed in the following section.

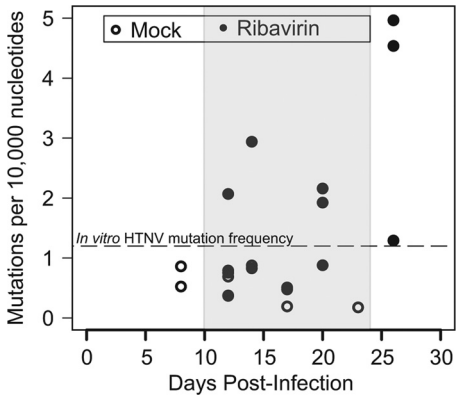

FIG 2 Average intrahost genetic variability of HTNV populations in mock- and ribavirin-treated mice. Mice were infected with 1,000 PFU of HTNV by intracranial injection on day 1. After 10 days, mock vehicle or ribavirin (50 mg/kg) was administered once per day for 14 days.

Ratio of nonsynonymous to synonymous substitution rates. Intrahost genetic variation of RNA viruses arises due to their intrinsically high mutation rates, resulting from error-prone replication (i.e., a lack of proofreading polymerase activity). It is constrained by purifying selection (also called negative selection), which eliminates new mutations that reduce specific infectivity relative to that of the ancestral sequence, for example, by decreasing the ability of an organism with a particular genotype to enter or replicate in a cell. Selection can also favor new genetic variants, as occurs, for example, *in vivo* when novel sequences allow escape from the host's immune response. Such selection favoring new variation is called positive selection. Whether or not selection is acting on a sequence and, if so, what type of selection is present can be detected by comparing the ratios of nonsynonymous to synonymous substitution rates (the *dN*/*dS* ratio).

To test for evidence of sites under positive or negative selection among sequences from mock- and ribavirin-treated, HTNV-infected mice, the coding regions of the nucleotide sequences were aligned using ClustalW and analyzed using the Datamonkey Web-

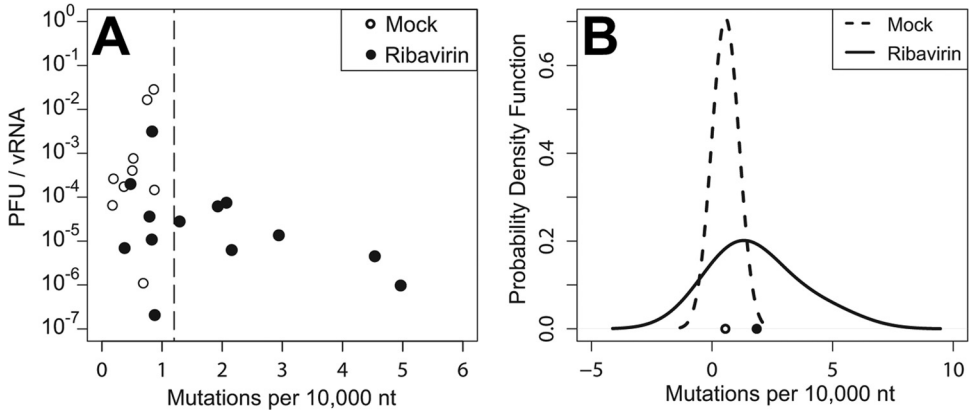

FIG 3 Selective infectivity of viruses from untreated and ribavirin-treated animals. (A) The mutation frequencies for individual animals from mock- and ribavirin-treated, infected groups were plotted against selective infectivity (number of PFU/vRNA copy). The hatched line represents the range of the starting HTNV seed stock material measured in Vero E6 cells *in vitro*. (B) Smoothed histograms (probability density functions) of vRNA mutation frequencies (numbers of mutations per 10,000 nt) in tissues of mock- and ribavirin-treated, HTNV-infected mice, showing that ribavirin-treated animals have a higher variance in mutation rate (Levene's test; $P = 0.067$). The smoothing bandwidths for the mock- and ribavirin-treated groups were 0.5 and 1.5, respectively.

based interface to the SLAC, FEL, IFEL, and FUBAR programs (39, 41). Each of these models uses different approaches to estimate the rates of *dN* and *dS* at each site. For example, SLAC is a counting method that may lack power for data sets comprising a small number of sequences or low divergence, such as in the mock-treated group (42), but it was included for comparison. Fixed-effects models such as FEL and IFEL directly estimate *dN* and *dS* at each site, in external and internal branches, respectively. The FUBAR method estimates the alignment-wide distribution of synonymous (α) and nonsynonymous (β) substitution rates, whose ratio (ω) is a common measure of the type of natural selection operating on the gene (ω values of <1 are interpreted as representing purifying selection, ω values of >1 represent pervasive diversifying selection, and ω values not statistically different from 1 represent neutral evolution) (39, 41). Having obtained this surface via Markov chain Monte Carlo sampling, it is then possible to apply an empirical Bayesian procedure to estimate the posterior distribution of ω at a given site, and thus to determine which sites are constrained and which ones are evolving adaptively.

The SLAC method did not detect any codons under positive or negative selection for either the mock- or ribavirin-treated group. FUBAR analyses detected three codons under pervasive purifying selection in the mock-treated group (codons 37, 193, and 225), and FEL analyses found the same three codons under negative selection in the mock-treated group (codons 37, 193, and 225). FEL also found, for the ribavirin-treated group, that codons 71 and 224 had two negatively selected sites. The IFEL and FUBAR analyses of the ribavirin-treated group (Table 4) found two sites with positive selection (A410 and P248) and two sites with pervasive diversifying selection (F165 and P248).

To explore the potential for episodic selection or a small number of branches subject to positive selection, we used MEME (43). MEME models variable ω values across lineages at an individual site (i.e., each site is treated as a fixed-effects component of the model). These analyses (Table 4) revealed two codons with episodic selection (F165 and P248) within the ribavirin-treated group, but none within the mock-treated group.

TABLE 3 Amino acid changes within Hantaan virus S segment in mice

Treatment group and mouse ID	dpi	Amino acid change(s)[a]
Mock-treated mice		
1007	8	E33G, R268Q, I325Fx2
1009	8	P182S
402	12	I20L, I109F, Q147R
404	12	V19E, D80Y, R282K
504	12	G63R, Q79H, G196D
308	14	ND
303	14	D110G
407	17	I122T
305	17	None
401	23	None
Ribavirin-treated mice		
1012	12	R26G, D37G, D59G, G99C, R156W, **A410E**
1013	12	Q55R, V84A
1201	12	Y265N, A291V, T318I, N423S
1105	14	A28T, K77R, M140I, K211E, E277G, L320M
1112	14	K30R, P174S, H176Y
1204	14	M95I, L120R, **F165R**, R267Q, S333F, A410G, D415N
1102	17	A208V, D394N
1209	20	G72R, M95I, D118N, A212V, L255F, A330V
1208	20	K41M, P132L, G204R, R263K
1207	20	A70T, K245R, E280D, R367K
1101	26	(A70V, G87E), D59N, E192K, R197K, A229V, E237G, P243S, I305T, A344V, D394N
1110	26	(R68K, P81L, L246F), (D88N, G99S, A288V), M188I, D167N, V130I, P182L, A227V, I193V, A260T, A260V, M295I, G310E, T318I, A387T
1109	26	S121N, T142I, R144K, S164L, Q196H, R199Kx3, C203Y, P218S, V222L, **P248S**, A251T, G257D, T278I, K358E, E425K

[a] Changes from wild-type HTNV 76-119 consensus sequence. Amino acids with detected positive or episodic selection are shown in bold. Changes in parentheses indicate concurrent mutations within a single genome. ND, none detected.

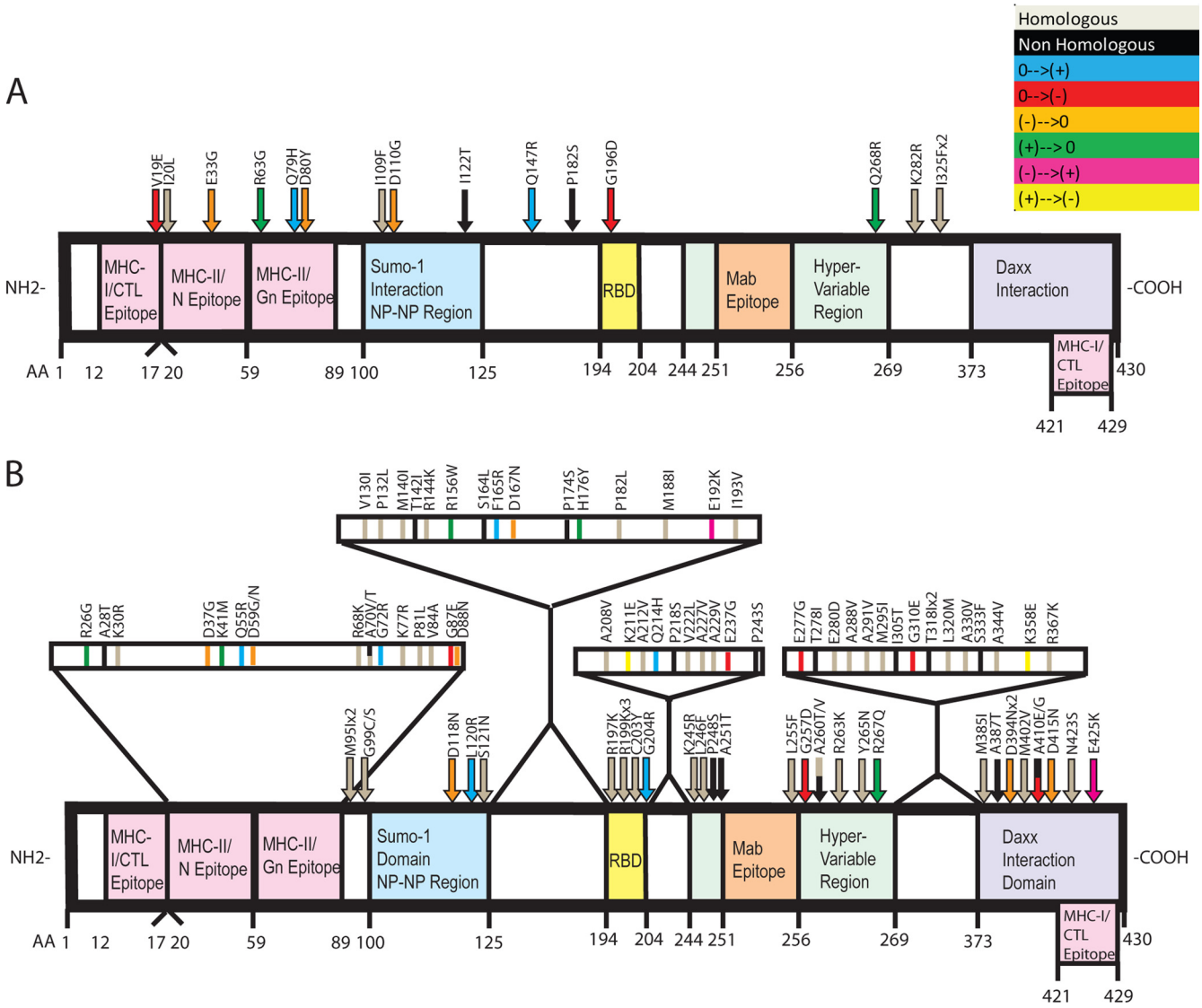

FIG 4 Illustration summarizing the locations of amino acid changes in the HTNV N protein. The amino acid changes from the HTNV wild-type N protein sequence identified in mock-treated (A) and ribavirin-treated (B), HTNV-infected mice are noted at the top. Corresponding colors reflect changes in amino acid charge. Functional domains within the N protein that have been identified in the literature are noted (57, 60–64).

DISCUSSION

Infection of hantaviruses can lead to persistence in one host without disease (rodent reservoir), acute infection with rapid clearance in another host (adult laboratory mice or wild, nonreservoir rodents), or lethal disease in yet another (humans or suckling mice). Upon accidental infection of humans, hantaviruses may cause two different illnesses in humans: HFRS and HPS (1, 4, 44). At present, there are no vaccines or antivirals available by the Food and Drug Administration for treatment of either disease. However, intravenous ribavirin has been used in clinical studies in China and Korea (13) for treatment of HFRS and HPS (45, 46). While the studies with HFRS show promise for ribavirin as a therapeutic approach, its use in treatment of HPS is as yet inconclusive. Efficacy studies in the lethal HPS hamster model of Andes virus infection suggest that it does have potential (47). Understanding ribavirin's mechanism of action and potential for selecting for drug resistance *in vitro* and *in vivo* is important to a full interpretation of its efficacy and safety for treatment of diseases caused by hantaviruses.

In this study, we employed a lethal murine model of hantaviral disease with a prototypic HFRS virus, HTNV, to gain insight into viral replication and genetic variation over time with and without ribavirin treatment. Our research and that of others have shown that small molecules such as ribavirin increase the mutation load of the viral genome, which results in the extinction of the virus *in vitro* (18, 27–30, 34). Improving our understanding of how to drive a virus to extinction by increasing genetic variation by use of small antiviral molecules such as ribavirin (e.g., lethal mutagenesis) requires insight into how viruses evolve and adapt within different environments. In naturally occurring infection cycles, changes in the standing genetic variation of viruses can arise during within-host (e.g., immune pressure, replication, and diversification) and between-host (e.g., transmission bottlenecks) pro-

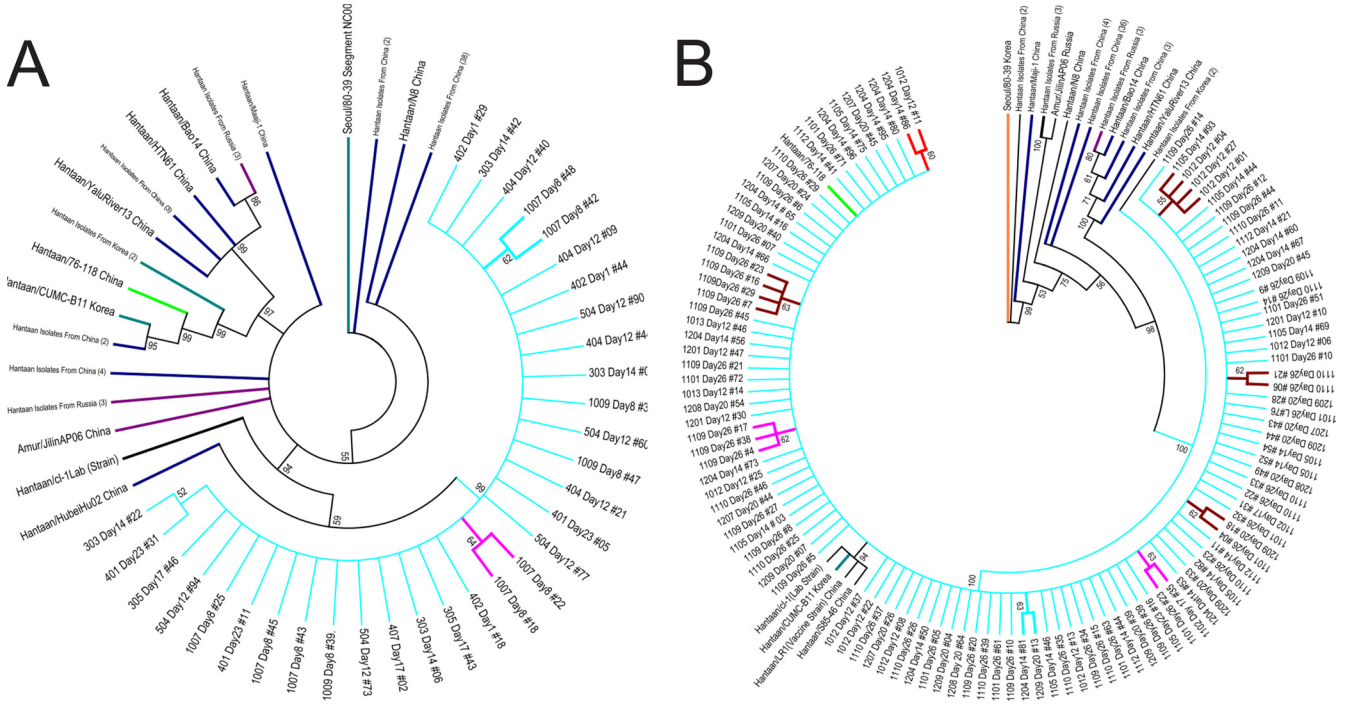

FIG 5 Maximum likelihood phylogenies of the open reading frame of the S-segment and wild-type HTNV sequences. Phylograms of nucleotide sequences from mock-treated (A) and ribavirin-treated (B), HTNV-infected mouse lungs are shown. The evolutionary history was inferred by using the maximum likelihood method based on the Tamura-Nei model (59). The tree with the highest log likelihood is shown for each data set. An initial tree(s) for the heuristic search was obtained automatically by applying neighbor-joining and BioNJ algorithms to a matrix of pairwise distances estimated using the maximum composite likelihood approach and then selecting the topology with the superior log likelihood value. Each tree is drawn to scale, with branch lengths measured in numbers of substitutions per site. Branches with amino acid substitutions are highlighted in pink, and those with positive selection are highlighted in red (A410). The analysis involved 180 nucleotide sequences. Codon positions included were 1st plus 2nd plus 3rd plus noncoding. All positions containing gaps and missing data were eliminated. There were a total of 1,233 positions in the final data set. Evolutionary analyses were conducted in MEGA 5.1 (37).

cesses of infection. Given the large population sizes and high mutation rates of RNA viruses, they are predicted to be enormously effective in their evolutionary response to natural selection. However, RNA viruses rarely show adaptive, positive selection in nature. This may be due to theoretical and experimental findings that suggest that many RNA viruses have evolved to replicate near their mutation threshold and hence have a relatively limited ability to explore the mutational space required for adaptation. Hence, the concept emerged to use mutagen-increasing small molecules such as ribavirin to increase the mutation load and cause error catastrophe or lethal extinction of the virus (18, 48–51). Error catastrophe is defined as a loss of genetic fidelity during RNA virus replication that results in a lethal accumulation of errors. Ribavirin increases the level of genetic variation or mutation load in hantaviruses, polioviruses, and others in the presence of ribavirin *in vitro*, resulting in error catastrophe or lethal extinction once a specific level of mutation is achieved by the drug (18, 27–30, 34). Therefore, one might predict that coupled with normal within-host selection processes, ribavirin would be even more effective in causing error catastrophe or lethal extinction of the virus *in vivo* than *in vitro*.

TABLE 4 Summary of MEME, IFEL, and FUBAR analyses

Analysis	Parameter	Value for amino acid identified[c]		
		F165	A410	P248
MEME[a]	α	5×10^{-6}	0	ND
	β	0	0	ND
	β+	10,000	3,627	ND
	P value	9.88×10^{-7}	0.0708	ND
IFEL	*dS*	ND	5×10^{-9}	5×10^{-9}
	dN	ND	78.60	95.09
	dN/*dS*	ND	15,720,120,000	19,017,460,000
	P value	ND	0.036374	0.0293944
FUBAR[b]	α	0.504806	ND	0.363532
	β	4.97696	ND	2.63544
	β > α	0.943738	ND	0.901973
	Empirical Bayes factor	17.7	ND	9.7

[a] Episodic diversifying selection. *P* values are based on Simes's procedure (significance level, 0.1).
[b] Pervasive diversifying selection at a posterior probability of ≥0.9.
[c] ND, none detected.

Our studies showed an elevation in mutation frequency of HTNV S-segment sequences in mice treated with ribavirin similar to that we previously reported for our *in vitro* studies (34, 35). We observed a corresponding decline in specific infectivity of HTNV over the course of infection in the ribavirin-treated mice, but we also observed a similar decline in untreated mice (Fig. 1). The biological bases for each were clearly different, since in the ribavirin-treated, HTNV-infected mice, we noted an increased mutational load and positive selection, while in the untreated mice, we

observed a decreased mutational load and purifying selection (Tables 2 to 4). Hence, while the difference in phenotype of the populations showed only a marginally significant *P* value (Fig. 1), significant changes occurred in the adaptation of the virus within the N protein (Table 4), in one evolutionary step (Fig. 4B versus Fig. 4A). Overall, the population data are consistent with the changes in selective infectivity (ability of a transcribed poliovirus RNA to produce infectious virus) reported for poliovirus in a direct test of the importance of mutation load *in vitro* (28). In that study, the ability of poliovirus RNA to produce infectious virus decreased with increased mutations, and the phenotype became lethal at a specific mutation load. Intriguingly, we found a decrease in diversity of the vRNA population in the untreated, HTNV-infected mice, rather than an increase in genetic diversity or selection of individual adaptive mutations that correlated with enhanced pathogenesis in the suckling mouse model.

We have few studies to compare our data with regarding the evolution of viruses in animal models of infection where animals are treated with ribavirin. Vignuzzi et al. reported an increase in genetic diversity which correlated with increased pathogenesis of poliovirus in a mouse model treated with ribavirin (52). Studies with foot-and-mouth disease virus (FMDV) showed that ribavirin-induced mutagenesis of an FMDV population *in vitro* resulted in attenuation of pathogenicity when these viruses were assessed by infection of an *in vivo* mouse model (53). Recently, coxsackie virus B3 has been shown to have a lower mutational robustness (greater sensitivity to ribavirin) than that of poliovirus (54). While direct comparison of the mutational robustness of HTNV to the values reported for poliovirus and coxsackievirus B3 is not possible, the values obtained *in vitro* and in this study are probably similar to or higher than those for poliovirus. The differences in the trajectories of these viruses may reflect unique solutions in their biological and evolutionary strategies for survival and adaptation during infection. For example, in contrast to hantaviruses, polioviruses have only one reservoir, humans, to maintain their reproductive rate, and FMDVs are maintained among cloven-hoofed animals as reservoirs. Among hantaviruses, human-to-human transmission has never been observed for HTNV and has been observed only for Andes virus, which is endemic in South America.

In addition to an elevated mutation load in ribavirin-treated mice, the average branch length is much longer in our phylogeny for ribavirin-treated, HTNV-infected mice (Fig. 4B) than in that for mock-treated mice, indicating that the changes induced by ribavirin can trigger longer evolutionary pathways. Numerous gain- or loss-of-negative-charge substitutions were revealed within the N protein (Table 3) and propagated in the sequence pool, suggesting a selective pressure of amino acids in the presence of ribavirin. Signatures of adaptation in these populations, while preliminary, suggest the importance of the viral N protein in the adaptive process. This is not surprising, since N is multifunctional and may interact with at least three host proteins. The N protein has the ability to interact with host cellular proteins to modulate immune signaling (55) and apoptosis (56). The N protein interacts with several host cellular proteins, such as Daxx, a Fas-mediated apoptosis enhancer (57), the ubiquitin-like modifier (SUMO-1), and ubiquitin-conjugating enzyme 9 (Ubc9) (58). The precise mechanism associated with these interactions involving N in the life cycle of the virus is as yet unknown.

HTNV populations from mock-treated and ribavirin-treated mice followed two different types of evolutionary trajectories, evolving under purifying and positive selection, respectively. Because our data indicate that virus populations in ribavirin-treated hosts have greater diversity, there are two non-mutually exclusive potential reasons for this difference. First, the difference in trajectories could be influenced by changes in selection experienced by the virus that were caused by ribavirin. For example, ribavirin may change the nature of the mouse immune response, resulting in different alleles, not present in the ancestor, being favored when HTNV finds itself in a ribavirin-treated host. Second, the difference in trajectories could be influenced by ribavirin's documented effect on the supply of new mutations. Increased mutation rates generated by exposure to ribavirin may give HTNV access to new, perhaps rare, alleles that would be beneficial in both treated and untreated hosts. Such universally beneficial alleles may exist because the HTNV used in this study is naive with regard to this suckling mouse model and may be far from its potential genetic optimum in this host. Regardless of the underlying selective cause, our experiments suggest that although the viruses within the ribavirin-treated, HTNV-infected mouse virus populations may suffer from a greater proportion of deleterious mutations, they harness the increased mutation rate to also achieve genetic changes that improve their survival over that of the wild type when exposed to a host treated with ribavirin.

In conclusion, the data presented herein suggest that ribavirin promotes a hypermutable environment that increases the mutation load in HTNV sequences in mice. Intriguingly, the levels of vRNA were similar in untreated and treated HTNV-infected mice, which suggests a potential benefit of increased mutational loads. Furthermore, the positive selection of amino acids in the N protein in the ribavirin-treated mice, but not the untreated mice, implies that ribavirin can also change the rate of adaptive evolution. In other words, sequence space not obtainable in untreated, HTNV-infected mice becomes available with ribavirin. With the increased availability of next-generation sequencing and reduced costs, future experiments will also capture other segments of the HTNV and hold promise to provide additional insights into evolutionary trajectories of additional virus-host interactions (entry-glycoprotein and polymerase-replication interactions). Experimental models of RNA viral evolution have largely been conducted within continuous cell lines in which viruses are well adapted and by creation of selection with temperature changes or small-molecule inhibitors of replication. *In vivo* approaches are a critical next step toward validation of these findings and to define the molecular mechanisms that influence zoonotic virus evolution and adaption in spillover hosts. In the specific case of ribavirin, the *in vivo* mouse model revealed positive selection of amino acids, while the *in vitro* studies did not. Future efforts will continue to explore the mechanisms of selection and adaptation of *Hantavirus in vivo* to not only promote an understanding of how to drive lethal extinction therapeutically but also provide insight into the molecular mechanisms that influence zoonotic virus evolution and adaption in reservoirs or spillover hosts.

ACKNOWLEDGMENTS

This work was supported in part by grants from the Department of Defense, USAMRC (grant W81XWH-04-C-0055), and the National Institutes of Health (R21 grant AI064499-01) to C.B.J.

We thank Blake Moore for technical assistance in conducting this study.

REFERENCES

1. **Jonsson CB, Figueiredo LT, Vapalahti O.** 2010. A global perspective on hantavirus ecology, epidemiology, and disease. Clin. Microbiol. Rev. **23:** 412–441.
2. **Schmaljohn CS, Hooper JW.** 2001. Bunyaviridae: the viruses and their replication, p 1581–1633. *In* Knipe DM, Howley PM, Griffin DE, Lamb RA, Martin MA, Roizman B, Straus SE (ed), Fields virology, 4th ed, vol 2. Lippincott Williams & Wilkins, Philadelphia, PA.
3. **Schmaljohn CS, Hasty SE, Harrison SA, Dalrymple JM.** 1983. Characterization of Hantaan virions, the prototype virus of hemorrhagic fever with renal syndrome. J. Infect. Dis. **148:**1005–1012.
4. **Peters CJ, Simpson GL, Levy H.** 1999. Spectrum of hantavirus infection: hemorrhagic fever with renal syndrome and hantavirus pulmonary syndrome. Annu. Rev. Med. **50:**531–545.
5. **Botten J, Mirowsky K, Ye C, Gottlieb K, Saavedra M, Ponce L, Hjelle B.** 2002. Shedding and intracage transmission of Sin Nombre hantavirus in the deer mouse (Peromyscus maniculatus) model. J. Virol. **76:**7587–7594.
6. **Ebihara H, Yoshimatsu K, Ogino M, Araki K, Ami Y, Kariwa H, Takashima I, Li D, Arikawa J.** 2000. Pathogenicity of Hantaan virus in newborn mice: genetic reassortant study demonstrating that a single amino acid change in glycoprotein G1 is related to virulence. J. Virol. **74:**9245–9255.
7. **Hutchinson KL, Rollin PE, Peters CJ.** 1998. Pathogenesis of a North American hantavirus, Black Creek Canal virus, in experimentally infected Sigmodon hispidus. Am. J. Trop. Med. Hyg. **59:**58–65.
8. **Lokugamage K, Kariwa H, Lokugamage N, Iwasa M, Hagiya T, Araki K, Tachi A, Mizutani T, Yoshimatsu K, Arikawa J, Iwasaki T, Takashima I.** 2004. Comparison of virulence of various hantaviruses related to hemorrhagic fever with renal syndrome in newborn mouse model. Jpn. J. Vet. Res. **51:**143–149.
9. **Hooper JW, Custer DM, Smith J, Wahl-Jensen V.** 2006. Hantaan/Andes virus DNA vaccine elicits a broadly cross-reactive neutralizing antibody response in nonhuman primates. Virology **347:**208–216.
10. **Hooper JW, Larsen T, Custer DM, Schmaljohn CS.** 2001. A lethal disease model for hantavirus pulmonary syndrome. Virology **289:**6–14.
11. **Huggins JW, Hsiang CM, Cosgriff TM, Guang MY, Smith JI, Wu ZO, LeDuc JW, Zheng ZM, Meegan JM, Wang QN, Oland DD, Gui XE, Gibbs PH, Yuan GH, Zhang TM.** 1991. Prospective, double-blind, concurrent, placebo-controlled clinical trial of intravenous ribavirin therapy of hemorrhagic fever with renal syndrome. J. Infect. Dis. **164:**1119–1127.
12. **Huggins JW, Kim GR, Brand OM, McKee KT, Jr.** 1986. Ribavirin therapy for Hantaan virus infection in suckling mice. J. Infect. Dis. **153:** 489–497.
13. **Rusnak JM, Byrne WR, Chung KN, Gibbs PH, Kim TT, Boudreau EF, Cosgriff T, Pittman P, Kim KY, Erlichman MS, Rezvani DF, Huggins JW.** 2009. Experience with intravenous ribavirin in the treatment of hemorrhagic fever with renal syndrome in Korea. Antiviral Res. **81:**68–76.
14. **Safronetz D, Ebihara H, Feldmann H, Hooper JW.** 2012. The Syrian hamster model of hantavirus pulmonary syndrome. Antiviral Res. **95:** 282–292.
15. **Bull JJ, Sanjuan R, Wilke CO.** 2007. Theory of lethal mutagenesis for viruses. J. Virol. **81:**2930–2939.
16. **Daifuku R.** 2003. Stealth nucleosides: mode of action and potential use in the treatment of viral diseases. BioDrugs **17:**169–177.
17. **Freistadt MS, Meades GD, Cameron CE.** 2004. Lethal mutagens: broad-spectrum antivirals with limited potential for development of resistance? Drug Resist. Updat. **7:**19–24.
18. **Jonsson CB, Milligan BG, Arterburn JB.** 2005. Potential importance of error catastrophe to the development of antiviral strategies for hantaviruses. Virus Res. **107:**195–205.
19. **Graci JD, Cameron CE.** 2006. Mechanisms of action of ribavirin against distinct viruses. Rev. Med. Virol. **16:**37–48.
20. **Leyssen P, Balzarini J, De Clercq E, Neyts J.** 2005. The predominant mechanism by which ribavirin exerts its antiviral activity in vitro against flaviviruses and paramyxoviruses is mediated by inhibition of IMP dehydrogenase. J. Virol. **79:**1943–1947.
21. **Malinoski F, Stollar V.** 1981. Inhibitors of IMP dehydrogenase prevent Sindbis virus replication and reduce GTP levels in Aedes albopictus cells. Virology **110:**281–289.
22. **Goswami BB, Borek E, Sharma OK, Fujitaki J, Smith RA.** 1979. The broad spectrum antiviral agent ribavirin inhibits capping of mRNA. Biochem. Biophys. Res. Commun. **89:**830–836.
23. **Toltzis P, Huang AS.** 1986. Effect of ribavirin on macromolecular synthesis in vesicular stomatitis virus-infected cells. Antimicrob. Agents Chemother. **29:**1010–1016.
24. **Eriksson B, Helgstrand E, Johansson NG, Larsson A, Misiorny A, Noren JO, Philipson L, Stenberg K, Stening G, Stridh S, Oberg B.** 1977. Inhibition of influenza virus ribonucleic acid polymerase by ribavirin triphosphate. Antimicrob. Agents Chemother. **11:**946–951.
25. **Fernandez-Larsson R, O'Connell K, Koumans E, Patterson JL.** 1989. Molecular analysis of the inhibitory effect of phosphorylated ribavirin on the vesicular stomatitis virus in vitro polymerase reaction. Antimicrob. Agents Chemother. **33:**1668–1673.
26. **Wray SK, Gilbert BE, Knight V.** 1985. Effect of ribavirin triphosphate on primer generation and elongation during influenza virus transcription in vitro. Antiviral Res. **5:**39–48.
27. **Crotty S, Cameron C, Andino R.** 2002. Ribavirin's antiviral mechanism of action: lethal mutagenesis? J. Mol. Med. (Berl.) **80:**86–95.
28. **Crotty S, Cameron CE, Andino R.** 2001. RNA virus error catastrophe: direct molecular test by using ribavirin. Proc. Natl. Acad. Sci. U. S. A. **98:**6895–6900.
29. **Cuevas JM, Gonzalez-Candelas F, Moya A, Sanjuan R.** 2009. Effect of ribavirin on the mutation rate and spectrum of hepatitis C virus in vivo. J. Virol. **83:**5760–5764.
30. **Vignuzzi M, Stone JK, Andino R.** 2005. Ribavirin and lethal mutagenesis of poliovirus: molecular mechanisms, resistance and biological implications. Virus Res. **107:**173–181.
31. **Tam RC, Pai B, Bard J, Lim C, Averett DR, Phan UT, Milovanovic T.** 1999. Ribavirin polarizes human T cell responses towards a type 1 cytokine profile. J. Hepatol. **30:**376–382.
32. **Kobayashi T, Nakatsuka K, Shimizu M, Tamura H, Shinya E, Atsukawa M, Harimoto H, Takahashi H, Sakamoto C.** 2012. Ribavirin modulates the conversion of human CD4(+) CD25(−) T cell to CD4(+) CD25(+) FOXP3(+) T cell via suppressing interleukin-10-producing regulatory T cell. Immunology **137:**259–270.
33. **Sun Y, Chung DH, Chu YK, Jonsson CB, Parker WB.** 2007. Activity of ribavirin against Hantaan virus correlates with production of ribavirin-5′-triphosphate, not with inhibition of IMP dehydrogenase. Antimicrob. Agents Chemother. **51:**84–88.
34. **Chung DH, Sun Y, Parker WB, Arterburn JB, Bartolucci A, Jonsson CB.** 2007. Ribavirin reveals a lethal threshold of allowable mutation frequency for Hantaan virus. J. Virol. **81:**11722–11729.
35. **Severson WE, Schmaljohn CS, Javadian A, Jonsson CB.** 2003. Ribavirin causes error catastrophe during Hantaan virus replication. J. Virol. **77:** 481–488.
36. **Takenaka A, Gibbs CJ, Jr, Gajdusek DC.** 1985. Antiviral neutralizing antibody to Hantaan virus as determined by plaque reduction technique. Arch. Virol. **84:**197–206.
37. **Tamura K, Peterson D, Peterson N, Stecher G, Nei M, Kumar S.** 2011. MEGA5: molecular evolutionary genetics analysis using maximum likelihood, evolutionary distance, and maximum parsimony methods. Mol. Biol. Evol. **28:**2731–2739.
38. **Schmaljohn CS, Jennings GB, Hay J, Dalrymple JM.** 1986. Coding strategy of the S genome segment of Hantaan virus. Virology **155:**633–643.
39. **Delport W, Poon AF, Frost SD, Kosakovsky Pond SL.** 2010. Datamonkey 2010: a suite of phylogenetic analysis tools for evolutionary biology. Bioinformatics **26:**2455–2457.
40. **Chung DH, Kumarapperuma SC, Sun Y, Li Q, Chu YK, Arterburn JB, Parker WB, Smith J, Spik K, Ramanathan HN, Schmaljohn CS, Jonsson CB.** 2008. Synthesis of 1-beta-D-ribofuranosyl-3-ethynyl-[1,2,4]triazole and its in vitro and in vivo efficacy against Hantavirus. Antiviral Res. **79:**19–27.
41. **Pond SL, Frost SD.** 2005. Datamonkey: rapid detection of selective pressure on individual sites of codon alignments. Bioinformatics **21:**2531–2533.
42. **Kosakovsky Pond SL, Frost SD.** 2005. Not so different after all: a comparison of methods for detecting amino acid sites under selection. Mol. Biol. Evol. **22:**1208–1222.
43. **Murrell B, Wertheim JO, Moola S, Weighill T, Scheffler K, Kosakovsky Pond SL.** 2012. Detecting individual sites subject to episodic diversifying selection. PLoS Genet. **8:**e1002764. doi:10.1371/journal.pgen.1002764.
44. **Schmaljohn C, Hjelle B.** 1997. Hantaviruses: a global disease problem. Emerg. Infect. Dis. **3:**95–104.
45. **Chapman LE, Mertz GJ, Peters CJ, Jolson HM, Khan AS, Ksiazek TG,**

Koster FT, Baum KF, Rollin PE, Pavia AT, Holman RC, Christenson JC, Rubin PJ, Behrman RE, Bell LJ, Simpson GL, Sadek RF. 1999. Intravenous ribavirin for hantavirus pulmonary syndrome: safety and tolerance during 1 year of open-label experience. Ribavirin Study Group. Antivir. Ther. **4:**211–219.
46. **Mertz GJ, Miedzinski L, Goade D, Pavia AT, Hjelle B, Hansbarger CO, Levy H, Koster FT, Baum K, Lindemulder A, Wang W, Riser L, Fernandez H, Whitley RJ.** 2004. Placebo-controlled, double-blind trial of intravenous ribavirin for the treatment of hantavirus cardiopulmonary syndrome in North America. Clin. Infect. Dis. **39:**1307–1313.
47. **Safronetz D, Haddock E, Feldmann F, Ebihara H, Feldmann H.** 2011. In vitro and in vivo activity of ribavirin against Andes virus infection. PLoS One **6:**e23560. doi:10.1371/journal.pone.0023560.
48. **Anderson JP, Daifuku R, Loeb LA.** 2004. Viral error catastrophe by mutagenic nucleosides. Annu. Rev. Microbiol. **58:**183–205.
49. **Crotty S, Maag D, Arnold JJ, Zhong W, Lau JY, Hong Z, Andino R, Cameron CE.** 2000. The broad-spectrum antiviral ribonucleoside ribavirin is an RNA virus mutagen. Nat. Med. **6:**1375–1379.
50. **Graci JD, Cameron CE.** 2002. Quasispecies, error catastrophe, and the antiviral activity of ribavirin. Virology **298:**175–180.
51. **Tam RC, Lau JY, Hong Z.** 2001. Mechanisms of action of ribavirin in antiviral therapies. Antivir. Chem. Chemother. **12:**261–272.
52. **Vignuzzi M, Stone JK, Arnold JJ, Cameron CE, Andino R.** 2006. Quasispecies diversity determines pathogenesis through cooperative interactions in a viral population. Nature **439:**344–348.
53. **Sanz-Ramos M, Rodriguez-Calvo T, Sevilla N.** 2012. Mutagenesis-mediated decrease of pathogenicity as a feature of the mutant spectrum of a viral population. PLoS One **7:**e39941. doi:10.1371/journal.pone.0039941.
54. **Graci JD, Gnadig NF, Galarraga JE, Castro C, Vignuzzi M, Cameron CE.** 2012. Mutational robustness of an RNA virus influences sensitivity to lethal mutagenesis. J. Virol. **86:**2869–2873.
55. **Taylor SL, Krempel RL, Schmaljohn CS.** 2009. Inhibition of TNF-alpha-induced activation of NF-kappaB by hantavirus nucleocapsid proteins. Ann. N. Y. Acad. Sci. **1171**(Suppl 1)**:**E86–E93.
56. **Ontiveros SJ, Li Q, Jonsson CB.** 2010. Modulation of apoptosis and immune signaling pathways by the Hantaan virus nucleocapsid protein. Virology **401:**165–178.
57. **Li XD, Makela TP, Guo D, Soliymani R, Koistinen V, Vapalahti O, Vaheri A, Lankinen H.** 2002. Hantavirus nucleocapsid protein interacts with the Fas-mediated apoptosis enhancer Daxx. J. Gen. Virol. **83:**759–766.
58. **Kaukinen P, Vaheri A, Plyusnin A.** 2003. Non-covalent interaction between nucleocapsid protein of Tula hantavirus and small ubiquitin-related modifier-1, SUMO-1. Virus Res. **92:**37–45.
59. **Tamura K, Nei M.** 1993. Estimation of the number of nucleotide substitutions in the control region of mitochondrial DNA in humans and chimpanzees. Mol. Biol. Evol. **10:**512–526.
60. **Jenison S, Yamada T, Morris C, Anderson B, Torrez-Martinez N, Keller N, Hjelle B.** 1994. Characterization of human antibody responses to Four Corners hantavirus infections among patients with hantavirus pulmonary syndrome. J. Virol. **68:**3000–3006.
61. **Lee BH, Yoshimatsu K, Maeda A, Ochiai K, Morimatsu M, Araki K, Ogino M, Morikawa S, Arikawa J.** 2003. Association of the nucleocapsid protein of the Seoul and Hantaan hantaviruses with small ubiquitin-like modifier-1-related molecules. Virus Res. **98:**83–91.
62. **Plyusnin A, Vapalahti O, Lankinen H, Lehvaslaiho H, Apekina N, Myasnikov Y, Kallio-Kokko H, Henttonen H, Lundkvist A, Brummer-Korvenkontio M.** 1994. Tula virus: a newly detected hantavirus carried by European common voles. J. Virol. **68:**7833–7839.
63. **Severson W, Xu X, Kuhn M, Senutovitch N, Thokala M, Ferron F, Longhi S, Canard B, Jonsson CB.** 2005. Essential amino acids of the Hantaan virus N protein in its interaction with RNA. J. Virol. **79:**10032–10039.
64. **Van Epps HL, Schmaljohn CS, Ennis FA.** 1999. Human memory cytotoxic T-lymphocyte (CTL) responses to Hantaan virus infection: identification of virus-specific and cross-reactive CD8(+) CTL epitopes on nucleocapsid protein. J. Virol. **73:**5301–5308.